Macromolecules

pubs.acs.org/Macromolecules Article

Understanding the Synthesis of Linear−Bottlebrush−Linear Block Copolymers: Toward Plastomers with Well-Defined Mechanical Properties

Yidan Cong, Mohammad Vatankhah-Varnosfaderani, Vahid Karimkhani, Andrew N. Keith, Frank A. Leibfarth, Michael R. Martinez, Krzysztof Matyjaszewski, and Sergei S. Sheiko*

Cite This: *Macromolecules* 2020, 53, 8324−8332 Read Online

ACCESS | Metrics & More | Article Recommendations | Supporting Information

ABSTRACT: Linear−bottlebrush−linear (LBL) triblock copolymers were synthesized via a two-step atom transfer radical polymerization (ATRP): (i) grafting-through polymerization of monomethacryloxypropyl-terminated poly(dimethylsiloxane) ($PDMS_{11}MA$) macromonomers, which yielded difunctional P($PDMS_{11}MA$) bottlebrush macroinitiators, followed by (ii) the growth of linear poly(methyl methacrylate) chains at both ends of the bottlebrush backbone. Upon microphase separation, LBL triblock copolymers self-assembled into thermoplastic elastomers (plastomers) that exhibited tissue-like mechanical properties controlled by triblock composition and architecture. The mechanical properties of plastomers obtained from different synthetic batches initially demonstrated variability due to the deleterious termination of chain ends, resulting in undesired side products, consisting of linear−brush diblocks and bottlebrush monoblocks in the final product. Therefore, the kinetics of grafting-through polymerization of $PDMS_{11}MA$ macromonomers was studied to establish correlations between reversible first-order kinetic trends and network mechanical properties. By varying the reaction conditions, including the initial monomer concentration, targeted degree of polymerization, and solvent, the syntheses of macroinitiators and chain extensions were optimized with improved chain-end fidelity while maintaining a high yield and provided elastomers with consistent desired mechanical properties.

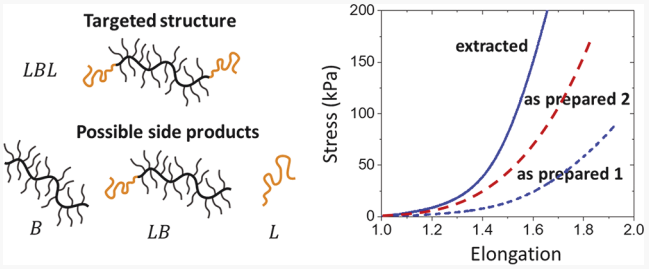

INTRODUCTION

The unique soft yet firm mechanical behavior of biological tissues is vital for the design of biomedical devices, soft robotics, and wearable electronics using synthetic materials.[1−5] The tissue stress−strain response includes two stages: a low-modulus elastic deformation at smaller strains followed by rapid stiffening and yielding at larger deformations.[5−9] Conventional synthetic elastomers and gels are able to recreate tissues' softness, but their strain-stiffening response is limited by entanglements of network strands.[2,10−12] To address this challenge, we introduced linear−bottlebrush−linear (LBL) triblock copolymers that microphase-separate to yield thermoplastic elastomers (or plastomers) (Figure 1a)[13] analogous to linear triblocks.[14−17] However, bottlebrush strands are architecturally disentangled and extended within LBL networks,[18−21] which generates a strong non-linear modulus increase with deformation.[18,22,25] Concurrently, microdomains of flexible linear blocks serve as hidden length reservoirs that unravel at larger deformations.[13,23,24] This oxymoronic combination of supersoft matrices composed of stiff brush macromolecules and hard microdomains composed of flexible linear chains creates the tissue-like stress−strain response (Figure 1b). Furthermore, specific mechanical properties, such as the Young's modulus (E_0), firmness (β), and elongation at break (λ_{max}) can be encoded into the LBL architecture by controlling the degrees of polymerization (DPs) of linear blocks (n_L), bottlebrush blocks (n_{bb}), and bottlebrush side chains (n_{sc}).[25] For example, altering n_L at a given B-block structure can create a wide range of mechanical responses (Figure 1c) that closely mimic those of soft biological tissues (Figure 1b). Although this material design platform promises revolutionary mechanics, it often faces batch-to-batch inconsistencies due to architectural impurities caused by imperfect synthesis. Favorably, the ability to measure the resulting mechanical properties provides a synthesis-mechanics feedback loop that readily detects these imperfections and thus can be utilized to instruct the development of detailed synthetic protocols.

To gain precise synthetic control of n_L and n_{bb}, we employed atom transfer radical polymerization (ATRP) to produce

Received: May 7, 2020
Revised: August 31, 2020
Published: September 25, 2020

https://dx.doi.org/10.1021/acs.macromol.0c01083
Macromolecules 2020, 53, 8324−8332

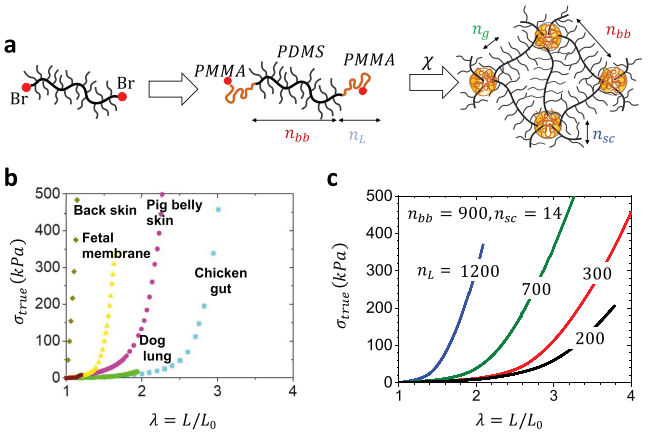

Figure 1. (a) Linear poly(methyl methacrylate) (PMMA) was grown from both ends of the poly(dimethylsiloxane) (PDMS) bottlebrush, resulting in linear−bottlebrush−linear triblock copolymers, which self-assemble into physical networks and resemble the mechanical properties of biological tissues. n_{bb}: DP of the P($PDMS_{11}MA$) bottlebrush, n_L: DP of the linear PMMA block on each end, n_g: grafting density of the P($PDMS_{11}MA$) bottlebrush, n_{sc}: side-chain length of the P($PDMS_{11}MA$) bottlebrush, and χ: Flory-Huggins interaction parameter. (b) Stress−elongation response of assorted biological tissues obtained by digitization of literature data (Table S1).[51−55] (c) Variation of the stress−elongation response of PMMA-*b*-P($PDMS_{11}MA$)-*b*-PMMA LBL plastomers (n_{bb} = 900, n_{sc} = 14) upon changing the degree of polymerization of the linear PMMA block as n_L = 200, 300, 700, 1200. Note: Reprinted with permission from ref 13. Copyright 2018 American Chemical Society.

polymers with narrow molecular weight distributions and well-defined architectures.[26,27] Despite this highly optimized method, chain-breaking events such as biradical termination or chain transfer remain a challenge when employing ATRP for grafting-through polymerization of macromonomers. Compared to small molecules, bulky macromonomers have slower rates of propagation and observable equilibrium monomer concentrations where the rate of propagation equals the rate of depropagation when [M] reaches its equilibrium monomer concentration, $[M]_e$. Polymerization does not occur when $[M]_0 < [M]_{eq}$.[28] The slow rate of polymerization, relative to the rates of chain-breaking reactions such as termination and transfer reactions, and the contribution of depolymerization could lead to a greater challenge in achieving both a high yield and chain-end functionality. The loss of chain-end functionality is detrimental to the synthesis of LBL triblock copolymers as it results in undesired linear−bottlebrush diblocks (LB) and bottlebrush homopolymer (B) impurities (Figure 2a). The effect of these impurities on the stress−strain response of LBL plastomers was demonstrated by varying polymerization conditions (Figure 2b). Plastomers with the same targeted chemical and architectural composition from two different batches demonstrated a significant difference in mechanical properties (Tables S3 and S4). Accordingly, comparison of two identical plastomers before and after extraction with hexane (Figure 2c) showed a significant stiffness increase after removal of free bottlebrushes (Tables S5 and S6), which were present between 25 and 29 wt % relative to the total yield of LBL plastomers (Table 1 and Figure S6). Conversely, we deliberately mixed P($PDMS_{11}MA$) bottlebrush homopolymers with triblock copolymers during network self-assembly to

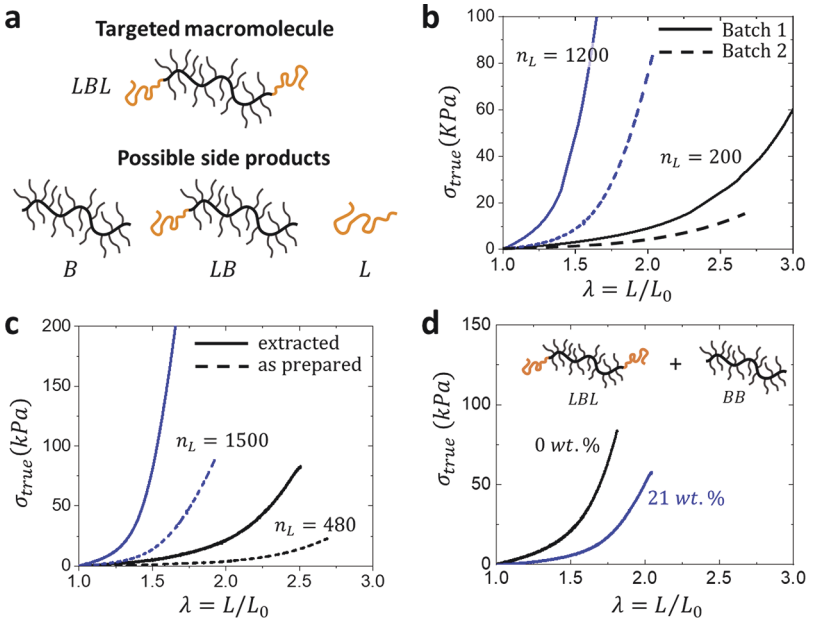

Figure 2. (a) Possible side products of LBL synthesis: bottlebrush homopolymer (B), linear-bottlebrush diblock (LB), linear PMMA homopolymer (L). (b) Two batches of two different plastomers, $PMMA_{1200}$-*b*-P($PDMSMA)_{900}$-*b*-$PMMA_{1200}$ (blue) and $PMMA_{200}$-*b*-P($PDMSMA)_{900}$-*b*-$PMMA_{200}$ (black), demonstrate significant variation of stress−elongation curves upon uniaxial extension at $\dot{\varepsilon}$ = 0.008 s^{-1}, T = 25 °C. For both batches, the initial macromonomer concentration was 0.4 M and the reaction was run in toluene at 45 °C (Experimental Section). Macroinitiator synthesis for batch 1 was quenched at 74% conversion, and that for batch 2 was quenched at 83% to reach the same P($PDMSMA)_{900}$ chain length. (c) Stress−elongation curves of two LBL plastomers, $PMMA_{1500}$-*b*-P($PDMSMA)_{940}$-*b*-$PMMA_{1500}$ (blue) and $PMMA_{480}$-*b*-P($PDMSMA)_{940}$-*b*-$PMMA_{480}$ (black), show a significant difference in stress−elongation response before (dashed lines) and after (solid lines) extraction of free B blocks from the plastomer samples. (d) Stress−elongation response changes upon adding 21 wt % free P($PDMS_{11}MA$) (n_{bb} = 860) bottlebrushes to $PBzMA_{540}$-*b*-P($PDMS_{11}MA)_{860}$-*b*-$PBzMA_{540}$ plastomers.

https://dx.doi.org/10.1021/acs.macromol.0c01083
Macromolecules 2020, 53, 8324−8332

Table 1. Free P(PDMS$_{11}$MA) Bottlebrushes Extracted from LBL Plastomers (Figure 2c)

n_{bb}	n_L	wt % P(PDMS$_{11}$MA) extracted
940[a]	480	25
	840	24
	1500	29

[a]Degree of polymerization of bottlebrush backbone after 83.3% on macromonomer conversion at a targeted n_{bb} = 1125.

demonstrate the plasticization effect on the stress−strain response (Figure 2d). A significant decrease in modulus (~3.5×) was observed after the addition of only 21 wt % P(PDMS$_{11}$MA) bottlebrushes (Table S7), which is counter to traditional network swelling theory[29] as the presence of free P(PDMS$_{11}$MA) significantly alters the LBL plastomer self-assembly pathway of the L-domains. Therefore, the mechanics of LBL, LB, and B mixtures warrants a future study that will investigate specific contributions of free brush fractions and their architectural dimensions (n_{sc}, n_g, and n_{bb}). Note that termination and chain transfer may also occur during linear block polymerization as observed by extractable linear homopolymers (Figure S7), but this does not significantly affect the resulting mechanical properties as (i) terminated LBLs are still mechanically active and average out over the entire network and (ii) free homopolymers constitute small fractions (2−4 wt %). To test the impurity hypothesis, we mixed linear homopolymers into purified triblocks during self-assembly. Their mechanical performance did not noticeably deviate from the pure triblock (Figure S8 and Table S2) and stresses the importance of minimizing termination and chain transfer in P(PDMS$_{11}$MA) polymerization.

Since the polymer network mechanics is sensitive to molecular structure, studying the mechanical properties of LBL plastomers prepared under systematically varied synthetic conditions enables assessing successful synthetic procedures. Taking advantage of both reaction kinetics and mechanical testing, we aimed to develop protocols to synthesize LBL triblocks with consistent mechanical properties so we can bridge chemical composition, architecture, and mechanics.

RESULTS AND DISCUSSION

Scheme 1 outlines the two-step synthesis of LBL copolymers. First, P(PDMS$_{11}$MA) bottlebrushes with Br-terminated chain ends were prepared by grafting-through polymerization of PDMS$_{11}$MA macromonomers with a difunctional ATRP initiator. After reaching the desired n_{bb}, the reaction was quenched and the bottlebrush solution was precipitated several times into methanol to remove unreacted macromonomers. The purified bottlebrush macroinitiators were then used to grow either linear PMMA or poly(benzyl methacrylate) (PBzMA) at both ends (complete synthetic details are in the Experimental Section and Supporting Information, Section S1). The typical dispersity of the bottlebrush macroinitiator and the corresponding LBL copolymer was $Đ \cong 1.5$ (Figure S4).

While the desired product was an LBL triblock copolymer, side products such as free bottlebrushes (B) and linear−bottlebrush diblock copolymers (LB) could also be produced as a result of deleterious termination or chain transfer reactions (Figure 2a). Due to the high molecular weight and similar solubility parameters, these side products are difficult to isolate by common purification techniques such as precipitation or dialysis; therefore, they could remain in the final materials and affect their mechanical properties. Hence, we systematically studied reaction conditions that could affect the kinetics of grafting-through polymerization of PDMS$_{11}$MA macromonomers, aiming to synthesize difunctional P(PDMS$_{11}$MA) macroinitiator brushes with a high $n_{bb} \approx 1000$, chain-end fidelity, and yield. Specifically, we explored the following synthetic parameters: (i) targeted DP of the bottlebrush backbone, (ii) initial monomer concentration, (iii) solvent type, and (iv) ATRP techniques.

In a typical synthesis, the PDMS$_{11}$MA macromonomer (MW = 1000 g/mol, n_{sc} = 14) was dissolved in toluene as a 0.4 M solution. Difunctional initiator ethylene bis(2-bromoisobutyrate) (2-BiB) was added according to the targeted DP, which was calculated by $[M]_0$:[I], along with $Cu^{(I)}Br$ and tris[2-(dimethylamino)ethyl]amine (Me_6TREN) where the molar equivalents of the catalyst and ligand relative to the initiator were [I]:[$Cu^{(I)}Br$]:[Me_6TREN] = 1:2:2 ([I] was calculated as the moles of 2-BiB divided by the volume of the reaction volume). The reaction temperature was kept at 45 °C for the duration of the polymerization. Kinetic aliquots were taken at different time points to determine conversion by ^1H NMR. The extent of termination in a grafting-through polymerization was assessed by deviation from a linear trend by a reversible first-order kinetic equation. This equation accounts for the reversibility in a grafting-through polymerization as [M] approaches the equilibrium monomer concentration $[M]_e$ of PDMS$_{11}$MA. When a polymerization reaches $[M]_e$, the rate of propagation is equal to the rate of depropagation and polymerization stops.[30−33] $[M]_e$ in a grafting-through polymerization is solvent and temperature-dependent.[34] The $[M]_e$ was estimated from the final monomer concentrations ($[M]_\infty$) of conventional radical polymerizations performed at $[M]_0$ =

Scheme 1. Two-Step Synthesis of Linear−Bottlebrush−Linear Triblock Copolymers with a P(PDMS$_{11}$MA) Bottlebrush Block and Linear PMMA Blocks at Both Ends[a]

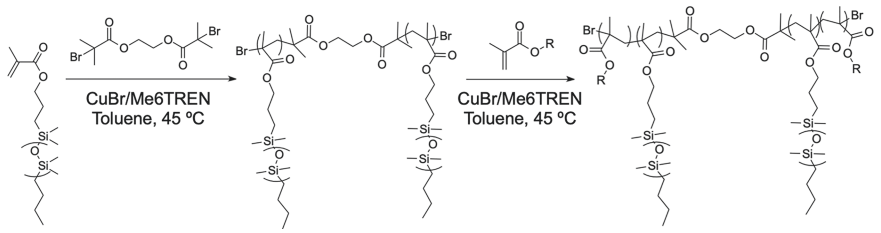

[a]Macromonomer PDMS$_{11}$MA has 11 Si atoms but totally 28 atoms (10 O atoms and 7 C atoms, forming a side chain). We use n_{sc} = 14 as the number of effective monomeric units per side chain by analogy with 14 vinyl monomeric units forming a chain with 28 atoms.

https://dx.doi.org/10.1021/acs.macromol.0c01083
Macromolecules 2020, 53, 8324−8332

100−400 mM.[35,36] (Supporting Information, Section S6). A decrease in the slope ($k_{p,app}$) of a kinetic plot for a reversible first order reaction can be attributed to a change in the radical concentration. In a normal ATRP, a decrease in the slope would correspond to an increase in [$CuBr_2$] due to radical termination according to the persistent radical effect.[37]

As shown in Figure 3a, a decrease in the rate of polymerization was observed at a lower conversion when targeting a higher DP of the bottlebrush backbone. Polymerizations that targeted an n_{bb} = 900 and 1200 exhibited a 10% decrease in the apparent rate of polymerization ($k_{p,app}$) at 85 and 70% conversion, respectively. Polymerization with a low targeted n_{bb} = 360 showed no noticeable decrease in $k_{p,app}$. Note that a higher targeted n_{bb} required a lower initiator and CuBr/Me_6TREN catalyst concentration. Control in a polymerization with only the CuBr/Me_6TREN activator will rely on radical termination to generate the $CuBr_2$/Me_6TREN deactivator, which can lead to a gradual improvement in polymerization control via a faster exchange reaction between active and dormant species but at the expense of lower chain-end functionality and polymerization rate.

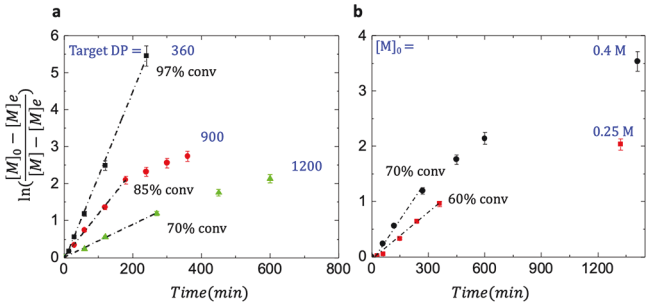

Figure 3. (a) Effect of target n_{bb} on the kinetics of grafting-through of $PDMS_{11}MA$ macromonomers. The initial concentration was 0.4 M. As the target DP increased, termination started to occur at a lower % conversion. (b) Effect of the initial monomer concentration on the kinetics of grafting-through of $PDMS_{11}MA$ macromonomers. The target n_{bb} was kept at 1200. As the initial monomer concentration decreased, termination started to occur at a lower % conversion. $[M]_e$ in toluene = 10 mM.

Next, the effect of the initial monomer concentration was investigated (Figure 3b). For the same targeted n_{bb} = 1200, a significant decrease in the polymerization rate occurred at lower conversions with a lower $[M]_0$. Specifically, 10% decreases in $k_{p,app}$ were observed after reaching 70 and 60% conversion for polymerizations conducted at $[M]_0$ = 0.40 and 0.25 M, respectively. From these studies, we concluded that the high chain-end functionality of $P(PDMS_{11}MA)$ can be improved by polymerization at a high initial monomer concentration, targeting lower conversion. This agrees with general rules for controlled radical polymerization.[38]

To verify the effect of chain-end fidelity on plastomer mechanical properties, we synthesized three batches of $P(PDMS_{11}MA)$ with the same final DP of n_{bb} = 850 ± 10, calculated as conversion × targeted n_{bb}. All three batches were synthesized using a 0.4 M initial monomer concentration. Batch 1 had a targeted n_{bb} = 1075, and the reaction was quenched at 80% conversion. The targeted backbone DP for batch 2 was 1200, and the reaction was quenched at 70% conversion. Finally, batch 3 had a targeted n_{bb} = 1600, and the reaction was quenched at 53% conversion. Using three different $P(PDMS_{11}MA)$ macroinitiators, a series of PBzMA-*b*-$P(PDMS_{11}MA)$-*b*-PBzMA triblocks with various n_L were synthesized. Films of each plastomer were prepared by slow solvent evaporation followed by tensile stress measurements. The measurement was performed three times for each sample. Figure 4a shows example stress−strain curves of LBL triblocks with the same n_{bb}, n_L, and n_{sc} using $P(PDMS_{11}MA)$ macroinitiators from batch 1, 2, and 3. The complete set of stress−strain curves of the three batches of plastomers as well as their corresponding mechanical parameters are included in Section S5 of the Supporting Information (Figures S9−S11 and Tables S8−S10). Despite similar compositions, plastomers assembled from these three triblocks exhibited different mechanical properties. To characterize the mechanical properties of plastomers, we used an equation of state,[39] which describes the relation between the true stress σ_{true} and deformation ratio $\lambda = L/L_0$.

$$\sigma_{true}/(\lambda^2 - \lambda^{-1}) = \frac{E}{9}\left(1 + 2\left(1 - \frac{\beta\left(\lambda^2 + \frac{2}{\lambda}\right)}{3}\right)^{-2}\right) \quad (1)$$

where E is the structural modulus and β is the firmness parameter ($\beta = \langle R_{in}^2\rangle/R_{max}^2$ where $\langle R_{in}^2\rangle$ is the mean square end-to-end distance between neighboring L-domains and R_{max} is the contour length of the bottlebrush backbone). The structural modulus E and firmness parameter β were obtained by fitting the true stress σ_{true} and deformation ratio λ from

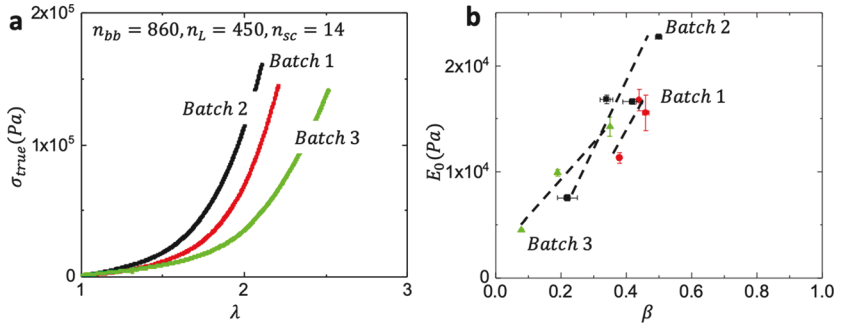

Figure 4. (a) Stress−strain curves of plastomers assembled from triblocks with the same architectural parameters (n_{bb} = 860, n_L = 450, and n_{sc} = 14) but synthesized using different batches of $P(PDMS_{11}MA)$ macroinitiators. (b) Young's modulus (E_0) vs the firmness parameter (β) for the three series of plastomers that were synthesized using the same $P(PDMS_{11}MA)$ macroinitiator from three different batches. Batch 1: targeted n_{bb} = 1075, % conversion = 80%. Batch 2: targeted n_{bb} = 1200, % conversion = 70%. Batch 3: targeted n_{bb} = 1600, % conversion = 53%.

https://dx.doi.org/10.1021/acs.macromol.0c01083
Macromolecules 2020, 53, 8324−8332

experimental data with eq 1. By substituting $\lambda = 1$ into the right-hand side of eq 1, we obtain the Young's modulus $E_0 = E(1 + 2(1 - \beta)^{-2})/9$. By plotting E_0 versus β, we compared the mechanical properties of three series of plastomers synthesized from different batches (Figure 4b). Each series consisted of 3–4 plastomers with different n_L values. The slope of batch 1 was approximately the same as batch 2, but the positions of batch 2 plastomers were above batch 1. Figure 4b suggests that plastomers synthesized using batch 2 macroinitiators are stiffer compared to batch 1 plastomers. This observation corroborated our hypothesis as reactions quenched at lower conversions (batch 2) lead to bottlebrushes with higher chain-end fidelity and less unfunctional BB impurities. However, a drop in the modulus and firmness was observed when the targeted n_{bb} was highest with batch 3. Batch 3 had the highest [M] relative to [2-BiB], which could lead to a lower $[Cu^{(II)}Br_2]$ concentration and poor deactivation. This suggests the need to balance the yield (batch 1) and $[Cu^{(II)}Br_2]$ concentration (batch 3) to improve chain-end fidelity and achieve optimal reaction conditions (batch 2), which are consistent with conventional ATRP kinetics.

The above experiments confirmed that lower chain-end fidelity of the bottlebrush macroinitiator affects the mechanical properties of plastomers. A primary cause of chain-end fidelity loss during radical polymerization could be radical termination or chain transfer of a growing polymer to monomer or to solvent. Generally, ATRP proceeds faster in polar solvents due to improved solubility of catalysts and an increase in K_{ATRP}.[40] In the case of the $PDMS_{11}MA$ macromonomer, polar solvent selection is limited because the nonpolar PDMS side chain has a particularly low Hildebrand solubility parameter of $\delta = 7.3$ $cal^{1/2}cm^{-3/2}$.[41] An ideal solvent for the grafting-through polymerization of $PDMS_{11}MA$ would have a large difference in the Hansen solubility parameter to limit thermodynamic barriers (increase the yield) while also having a low transfer coefficient.[33] Transfer of a H-atom from solvent to a growing polymer radical can become important at high monomer conversion where the rate of propagation is low due to a low [M], while the concentrations of the growing radical polymer chain ([P*]) and H-atom capped solvent ([S-H]) remain high. This can slow a polymerization if the solvent-derived dormant species (for example, benzyl bromide formed from toluene) is much less ATRP-active (has a ca. 2 orders of magnitude-lower k_{act}) than the dormant $P(PDMS_{11}MA)$-Br polymer chain.[42−44]

tert-Butylbenzene and chlorobenzene were assessed as solvents for $PDMS_{11}MA$ polymerization due to their anticipated lower transfer coefficients collected from the literature (Table S11). Both solvents have similar solubility profiles to toluene but lack functional groups with readily extractable benzylic protons. Polymerization of $PDMS_{11}MA$ in tetrahydrofuran (THF) exhibited an earlier decrease in $k_{p,app}$ relative to toluene and was not investigated further (Figure S13).

Polymerizations were run in three different solvents (toluene, *tert*-butylbenzene, and chlorobenzene) under the same $[M]_0 = 0.4$ M, targeted $n_{bb} = 1200$, and $[I]:[Cu^{(I)}Br]:[Me_6TREN] = 1:2:2$ ([I] was calculated as the mole of 2-BiB divided by the volume of the reaction volume). Comparison of the reversible first-order kinetic plots shows that reactions in *tert*-butylbenzene and chlorobenzene proceeded to >90% conversion before a significant decrease in $k_{p,app}$ was observed, while polymerization in toluene gradually slowed after reaching 70% conversion (Figure 5). This systematic study suggested

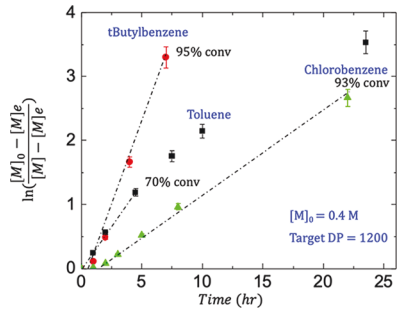

Figure 5. Comparison of reaction kinetics in different solvents. All reactions were run at 45 °C, and the initial monomer concentration was 0.4 M. The targeted DP of the bottlebrush backbone was $n_{bb} = 1200$ and $[I]:[Cu^{(I)}]:[Me_6TREN] = 1:2:2$. For the reactions that occurred in *tert*-butylbenzene and chlorobenzene, termination occurred after the conversion reached 90%, while termination started to occur at 70% conversion for the reaction in toluene. $[M]_e$ in toluene = 10 mM. $[M]_e$ in *tert*-butylbenzene = 5 mM.

that solvent choice is important in maintaining the chain-end functionality of $P(PDMS_{11}MA)$ bottlebrushes. Using solvents such as *tert*-butylbenzene and chlorobenzene, we were able to avoid the formation of solvent-derived dormant species, which would slow polymerization, as well as maintain an efficient rate of ATRP. Hence, this modification in solvents provided a more reliable method of synthesizing $P(PDMS_{11}MA)$ bottlebrushes with high chain-end fidelity.

Another approach to decrease the probability of chain-breaking reactions during grafting-through polymerization of $PDMS_{11}MA$ macromonomers is to improve catalytic systems. To extend the livingness of controlled radical polymerization as well as decrease the amount of catalysts used, several alternatives to the traditional ATRP methods such as activators regenerated by electron transfer (ARGET) ATRP, initiators for continuous activator regeneration (ICAR) ATRP, eATRP, and photoinduced ATRP were recently developed.[45] In our study, we selected a supplemental activator and reducing agent (SARA) ATRP technique.[46] SARA ATRP is a subset of ARGET ATRP where $Cu^{(0)}$ is used as a reducing agent but it can also serve as a supplemental activator for halogen-terminated initiators and polymer chain ends. $Cu^{(0)}$ can comproportionate with $Cu^{(II)}$ to produce two equivalents of $Cu^{(I)}$, while in the reverse process, two equivalents of $Cu^{(I)}$ disproportionate to one equivalent of Cu(0) and one equivalent of $Cu^{(II)}$ (Scheme 2).[47] The benefits of using SARA ATRP include a lower catalyst loading, a higher concentration of deactivating $Cu^{(II)}$ species, and lower sensitivity to oxygen.

In this study, a copper wire with a 1 mm diameter was used as the source of $Cu^{(0)}$, the initial $PDMS_{11}MA$ macromonomer

Scheme 2. Mechanism of SARA ATRP

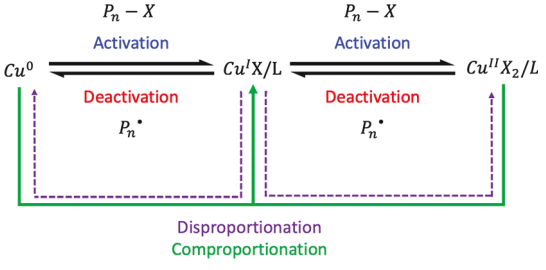

https://dx.doi.org/10.1021/acs.macromol.0c01083
Macromolecules 2020, 53, 8324−8332

concentration was 0.40 M, and [I]:[$Cu^{(II)}Br_2$]:[Me_6TREN] = 1:0.1:2. In order for the reaction to proceed more efficiently, solvent effects should also be taken into account. One of the factors that affect the rate of SARA ATRP is the rate at which $Cu^{(I)}$ is extracted from the surface of $Cu^{(0)}$ and dissolved in solution.[48] Here, tetrahydrofuran (THF) was investigated in SARA ATRP in comparison to toluene used in traditional ATRP. The targeted backbone DP for both experiments was n_{bb} = 1200. As seen in Figure 6, appreciable termination was

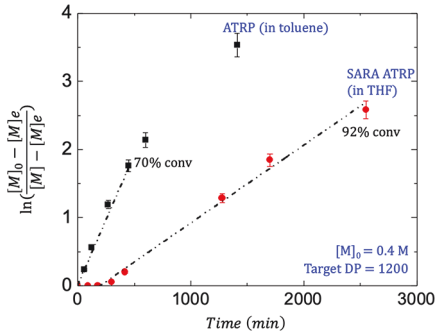

Figure 6. Comparison between traditional ATRP and SARA ATRP. Targeted n_{bb} = 1200, [$Cu^{(0)}$] = 0.08 cm^2/mL, [$Cu^{(II)}$] = 10 mol%, and [$Cu^{(II)}Br_2$]:[Me_6TREN] = 1:20. The initial monomer concentration was 0.4 M for both reactions, and the temperature was set to 45 °C. In toluene, $[M]_e$ = 10 mM.

observed after 70% conversion for the reaction using normal ATRP. However, SARA ATRP was able to achieve 92% conversion at which the reaction was quenched before the rate decrease started to occur. There was also an induction period of >5 h in the kinetic plot in SARA ATRP. Note that, although $Cu^{(0)}$ itself can act as an activator, the activating efficiency is significantly lower than that of $Cu^{(I)}$.[46] Furthermore, as shown in Figure 6, the reactions in SARA ATRP were threefold slower compared to the traditional ATRP method. This was expected due to the induction period as well as more $Cu^{(II)}$ in the system causing the deactivation rate to be faster; hence, the overall rate of ATRP was slower and accompanied by less termination.[49]

CONCLUSIONS

In this study, we demonstrated that the unique tissue-mimetic plastomer platform is sensitive to synthetic impurities caused by loss of chain-end functionality during macromonomer polymerization, which elucidates observed discrepancies in the mechanical properties of plastomers with similar architecture targets. Grafting-through polymerization of PDMSMA is challenging due to the limited selection of solvents, which are not prone to chain-breaking reactions, and a slow rate of propagation, which is in competition with depropagation.[50] We were able to provide synthetic insights to overcome the challenges to prepare difunctional P($PDMS_{11}$MA) macroinitiators with high chain-end fidelity.

In particular, we performed kinetic studies of grafting-through polymerization of a $PDMS_{11}$MA macromonomer under systematically different conditions. Kinetic studies showed that chain-breaking reactions can become significant in polymerizations conducted at low initial monomer concentrations in solvents with high transfer coefficients. Increasing the macromonomer concentration, targeting higher polymerization DP, and stopping polymerization at lower conversion decreased the extent of terminated chains. Polymerization in *tert*-butylbenzene and chlorobenzene had better polymerization control due to a decreased rate of chain transfer reactions compared to toluene. Additionally, SARA ATRP was successful in synthesizing P($PDMS_{11}$MA) with a high targeted backbone DP and chain-end fidelity. In conclusion, the best synthetic conditions to minimize LB and B impurities were as follows: (1) $[M]_o$ > 0.4 M, (2) solvents without moieties to undergo chain transfer reactions, such as *tert*-butylbenzene and chlorobenzene, and (3) methods that produce a higher-fraction $CuBr_2$/L deactivating catalyst without relying on RT, such as SARA ATRP.

Additionally, we developed a novel method to qualitatively assess loss of chain-end functionality in macromonomer polymerization by the mechanical properties of final LBL triblocks. All of these efforts will facilitate future LBL triblock design to achieve robust and consistent mechanical properties.

EXPERIMENTAL SECTION

Materials. Monomethacryloxypropyl-terminated poly(dimethylsiloxane) (MCR-M11, average molar mass ∼ 1000 g/mol, effective side-chain degree of polymerization (DP) n_{sc} = 14 (Figure S2), and dispersity Đ = 1.15 determined previously by GPC) was obtained from Gelest. Methyl methacrylate (MMA, 99%) was obtained from Acros. As explained in Scheme 1, the coding of the macromonomer name $PDMS_{11}$MA corresponds to 11 Si atoms in a side chain. However, the side chain contains totally 28 atoms (11 Si atoms, 10 O atoms, and 7 C atoms). Therefore, for consistency with previous reports, we use n_{sc} = 14 as the number of effective monomeric units per side chain by analogy with 14 vinyl monomeric units forming a chain with 28 atoms. Benzyl methacrylate (BzMA, 96%) was obtained from Sigma Aldrich. All monomers were purified by passing through basic alumina columns to remove inhibitors. A copper wire (1 mm in diameter) was purchased from VWR Scientific. The wire was immersed in hydrochloric acid/methanol (50/50 v/v%) to remove the copper oxide coating prior to usage. $Copper^{(I)}$ bromide (CuBr, ≥99.995%), $copper^{(II)}$ bromide ($CuBr_2$, ≥99.995%), tris[2-(dimethylamino)ethyl]amine (Me_6TREN), tetrahydrofuran (THF), toluene, *tert*-butylbenzene, and hexane were purchased from Sigma-Aldrich and used as received. Ethylene bis(2-bromoisobutyrate) (2-BiB) was synthesized following the procedure in Section S1.2.[56]

Instrumentation. A Brüker 400 MHz spectrometer was used to measure nuclei magnetic resonance (NMR) spectra of polymers. TRIOS RSA-G2 4020-0220 dynamic mechanical analysis (DMA) was used to perform tensile stress measurements of plastomer films. The imaging was performed in the PeakForce QNM mode using a multimode AFM (Brüker) with a NanoScope V controller and silicon probes (resonance frequency of 50−90 Hz and a spring constant of ∼0.4 N/m). A Tosoh EcoSEC Elite GPC system with refraction index (RI) and multi-angle light scattering (MALS) detectors were used to characterize the dispersity of the materials. Tetrahydrofuran (THF) was used as the solvent.

General Procedure for Grafting-Through Polymerization of the $PDMS_{11}$MA Bottlebrush. $PDMS_{11}$MA and toluene were added to a 50 mL Schlenk flask charged with a stir bar. The 2-BiB initiator and Me_6TREN, at a ratio of [I]:[Me6TREN] = 1:2, were added to the flask. The mixture was degassed for 1.5 h under nitrogen, and copper(I) bromide ([I]:[CuBr] = 1:2) was quickly added to the Schlenk flask. The reaction mixture was degassed for another 5 min before immersing into a 45 °C oil bath. Aliquots were extracted from the reaction solution during certain time intervals to monitor the kinetics of the reaction. The reaction was allowed to continue until the desired percent conversion was reached. The reaction was then quenched by air and washed with methanol six times to remove unreacted macromonomers.

General Procedure for SARA ATRP of the $PDMS_{11}$MA Bottlebrush. The $PDMS_{11}$MA macromonomer and THF were added to a 50 mL Schlenk flask charged with a stir bar. $CuBr_2$, the 2-

https://dx.doi.org/10.1021/acs.macromol.0c01083
Macromolecules 2020, 53, 8324−8332

BiB initiator, and Me_6TREN, at a ratio of [$CuBr_2$]:[I]:[Me_6TREN] = 0.1:1:10, were added into the flask. The mixture was degassed for 1.5 h under nitrogen. A 9 cm copper wire, washed with 50 vol % HCl in methanol, was quickly added to the Schlenk flask. The reaction mixture was degassed for another 5 min before immersing into a 45 °C oil bath. Aliquots were extracted from the reaction solution during certain time intervals to monitor the kinetics of the reaction. The reaction was allowed to continue until the desired percent conversion was reached. The reaction was then quenched by air and washed with methanol six times to remove unreacted macromonomers.

General Procedure for Chain Extension of the BB $PDMS_{11}MA$ Bottlebrush Macroinitiator. To prepare L−B−L triblock copolymers, synthesized and purified $PDMS_{11}MA$ bottlebrushes were used as macroinitiators to grow linear methacrylate side blocks at both ends. Here, we use poly(benzyl methacrylate)-*b*-P($PDMS_{11}MA$)-*b*-poly(benzyl methacrylate) (PBzMA-*b*-P($PDMS_{11}MA$)-*b*-PBzMA) as an example. In a typical synthesis, 5.44 g of the P($PDMS_{11}MA$) macroinitiator (n_{bb} = 860, 6.33 μmol), 5 g of BzMA (280 mM), 6.6 μL of Me_6TREN (25 μmol), and 30 mL of toluene were added to a 100 mL Schlenk flask equipped with a stir bar. The solution was degassed by nitrogen gas for 1.5 h then 3.6 mg of CuBr (5 μmol) was quickly added to the Schlenk flask, and the reaction mixture was then degassed for another 5 min. The flask was immersed in a 45 °C oil bath until the desired conversion was reached (verified by ^{1}H NMR). The reaction was then quenched by exposure to air and dried. The crude product was dissolved in DCM and precipitated in methanol three times to remove unreacted BzMA monomers and copper catalysts. The pure products were dried with airflow to remove DCM and methanol and vacuumed overnight. The DP and mass ratio of linear end bocks were measured by ^{1}H NMR ($CDCl_3$, Brüker 400 MHz spectrometer) (Figure S3). Using the same method described above, poly(methyl methacrylate)-*b*-P($PDMS_{11}MA$)-*b*-poly(methyl methacrylate) (PMMA-*b*-P($PDMS_{11}MA$)-*b*-PMMA) was synthesized (Figure S5).

Extraction of the Free P($PDMS_{11}MA$) Bottlebrush from LBL Triblock Copolymers. The triblock copolymer samples were dissolved in THF and precipitated into hexane three times to extract poly(dimethylsiloxane) bottlebrushes. The extracted content was dried and its chemical composition was characterized by ^{1}H NMR (Figure S6).

General Procedure of Tensile Stress Experiments. LBL triblocks were dissolved in toluene, resulting in a 25 wt % solution. The solution was poured into a Teflon mold, and the solution was dried by slow evaporation. The dried film was carefully removed from the mold and cut into a dog-bone shape. The dog-bone-shaped film was then loaded onto the DMA instrument. Uniaxial extension was performed at $\dot{\varepsilon}$ = 0.008 s^{-1}, T = 25 °C.

■ ASSOCIATED CONTENT

Supporting Information

The Supporting Information is available free of charge at https://pubs.acs.org/doi/10.1021/acs.macromol.0c01083.

Synthesis and characterization bottlebrush macroinitiators and linear−brush−linear (LBL) block copolymers, extraction of free bottlebrushes from LBL plastomers, stress−elongation responses and mechanical properties of LBL plastomers, polymerization kinetics, and equilibrium macromonomer concentration measurements (PDF)

■ AUTHOR INFORMATION

Corresponding Author

Sergei S. Sheiko − *Department of Chemistry, University of North Carolina, Chapel Hill, North Carolina 27599-3220, United States;* orcid.org/0000-0003-3672-1611; Email: sergei@email.unc.edu

Authors

Yidan Cong − *Department of Chemistry, University of North Carolina, Chapel Hill, North Carolina 27599-3220, United States;* orcid.org/0000-0002-8675-4780

Mohammad Vatankhah-Varnosfaderani − *Department of Chemistry, University of North Carolina, Chapel Hill, North Carolina 27599-3220, United States;* orcid.org/0000-0001-7636-9099

Vahid Karimkhani − *Department of Chemistry, University of North Carolina, Chapel Hill, North Carolina 27599-3220, United States;* orcid.org/0000-0003-0668-8814

Andrew N. Keith − *Department of Chemistry, University of North Carolina, Chapel Hill, North Carolina 27599-3220, United States;* orcid.org/0000-0001-6351-5392

Frank A. Leibfarth − *Department of Chemistry, University of North Carolina, Chapel Hill, North Carolina 27599-3220, United States;* orcid.org/0000-0001-7737-0331

Michael R. Martinez − *Department of Chemistry, Carnegie Mellon University, Pittsburgh, Pennsylvania 15213, United States;* orcid.org/0000-0002-6211-763X

Krzysztof Matyjaszewski − *Department of Chemistry, Carnegie Mellon University, Pittsburgh, Pennsylvania 15213, United States;* orcid.org/0000-0003-1960-3402

Complete contact information is available at: https://pubs.acs.org/10.1021/acs.macromol.0c01083

Notes

The authors declare no competing financial interest.

■ ACKNOWLEDGMENTS

The authors gratefully acknowledge funding from the National Science Foundation (nos. DMR 2004048, DMR 1921835, and DMR 1921858).

■ REFERENCES

(1) So, J.-H.; Tayi, A. S.; Güder, F.; Whitesides, G. M. Stepped moduli in layered composites. *Adv. Funct. Mater.* **2014**, *24*, 7197−7204.

(2) Martinez, R. V.; Glavan, A. C.; Keplinger, C.; Oyetibo, A. I.; Whitesides, G. M. Soft actuators and robots that are resistant to mechanical damage. *Adv. Mater.* **2014**, *24*, 3003−3010.

(3) Vatankhah-Varnoosfaderani, M.; et al. Bottlebrush elastomers: a new platform for freestanding electroactuation. *Adv. Mater.* **2017**, *29*, 1604209.

(4) Trung, T. Q.; Ramasundaram, S.; Hwang, B.-U.; Lee, N.-E. An all-elastic transparent and stretchable temperature sensor for body-attachable wearable electronics. *Adv. Mater.* **2016**, *28*, 502−509.

(5) Storm, C.; Pastore, J. J.; MacKintosh, F. C.; Lubensky, T. C.; Janmey, P. A. Nonlinear elasticity in biological gels. *Nature* **2005**, *435*, 191−194.

(6) Greenleaf, J. F.; Fatemi, M.; Insana, M. Selected methods for imaging elastic properties of biological tissues. *Annu. Rev. Biomed. Eng.* **2003**, *5*, 57−78.

(7) Demiray, H. A note on the elasticity of soft biological tissues. *J. Biomech.* **1972**, *5*, 309−311.

(8) Minns, R. J.; Soden, P. D.; Jackson, D. S. The role of the fibrous components and ground substance in the mechanical properties of biological tissues: a preliminary investigation. *J. Biomech.* **1973**, *6*, 153−165.

(9) Gosline, J.; et al. Elastic proteins: biological roles and mechanical properties. *Phil. Trans. R. Soc. Lond.* **2002**, *357*, 121−132.

(10) Ranzani, T.; Gerboni, G.; Cianchetti, M.; Menciassi, A. A bioinspired soft manipulator for minimally invasive surgery. *Bioinspir. Biomim.* **2015**, *10*, No. 035008.

(11) Lee, J.; Macosko, C. W.; Urry, D. W. Mechanical properties of cross-linked synthetic elastomeric polypentapeptides. *Macromolecules* **2001**, *34*, 5968−5974.
(12) Vatankhah-Varnosfaderani, M.; et al. Mimicking biological stress-strain behaviour with synthetic elastomers. *Nature* **2017**, *549*, 497−501.
(13) Vatankhah-Varnosfaderani, M.; et al. Chameleon-like elastomers with molecularly encoded strain-adaptive stiffening and coloration. *Science* **2018**, *359*, 1509−1513.
(14) Yu, J. M.; Dubois, P.; Teyssié, P.; Jérôme, R. Syndiotactic Poly(methyl methacrylate)(sPMMA)-Polybutadiene (PBD)-sPMMA Triblock Copolymers: Synthesis, Morphology, and Mechanical Properties. *Macromolecules* **1996**, *29*, 6090−6099.
(15) Honeker, C. C.; Thomas, E. L. Impact of Morphological Orientation in Determining Mechanical Properties in Triblock Copolymer Systems. *Chem. Mater.* **1996**, *8*, 1702−1714.
(16) Erk, K. A.; Henderson, K. J.; Shull, K. R. Strain Stiffening in Synthetic and Biopolymer Networks. *Biomacromolecules* **2010**, *11*, 1358−1363.
(17) Watts, A.; Kurokawa, N.; Hillmyer, M. A. Strong, resilient and sustainable aliphatic polyester thermoplastic elastomers. *Biomacromolecules* **2017**, *18*, 1845−1854.
(18) Bolton, J.; Rzayev, J. Synthesis and melt self-assembly of PS−PMMA−PLA triblock bottlebrush copolymers. *Macromolecules* **2014**, *47*, 2864−2874.
(19) Verduzco, R.; Li, X.; Pesek, S. L.; Stein, G. E. Structure, function, self-assembly, and applications of bottlebrush copolymers. *Chem. Soc. Rev.* **2015**, *44*, 2405−2420.
(20) Bates, C. M.; Chang, A. B.; Momčilović, N.; Jones, S. C.; Grubbs, R. H. ABA Triblock Brush Polymers: Synthesis, Self-Assembly, Conductivity, and Rheological Properties. *Macromolecules* **2015**, *48*, 4967−4973.
(21) Müllner, M.; Müller, A. H. E. Cylindrical polymer brushes - anisotropic building blocks, unimolecular templates and particle nanocarriers. *Polymer* **2016**, *98*, 389−401.
(22) Zhang, J.; Wang, Z.; Wang, X.; Wang, Z. The synthesis of bottlebrush cellulose-*graft*-diblock copolymer elastomers *via* atom transfer radical polymerization utilizing a halide exchange technique. *Chem. Commun.* **2019**, *55*, 13904−113907.
(23) Fantner, G. E.; et al. Sacrificial bonds and hidden length: Unraveling molecular mesostructures in tough materials. *Biophys. J.* **2006**, *90*, 1411−1418.
(24) Keith, A. N.; et al. Bottlebrush bridge between soft gels and firm tissues. *ACS Cent. Sci.* **2020**, *6*, 413−419.
(25) Sheiko, S. S.; Dobrynin, A. V. Architectural Code for Rubber Elasticity: From Supersoft to Superfirm Materials. *Macromolecules* **2019**, *52*, 7531−7546.
(26) Wang, J. S.; Matyjaszewski, K. Controlled/ "living" radical polymerization. Atom transfer radical polymerization in the presence of transition-metal complexes. *J. Am. Chem. Soc.* **1995**, *117*, 5614−5615.
(27) Matyjaszewski, K. Advanced materials by atom transfer radical polymerization. *Adv. Mater.* **2018**, *30*, 1706441.
(28) Leonard, J. Thermodynamics of equilibrium polymerization in solution. Effect of polymer concentration on the equilibrium monomer concentration. *Macromolecules* **1969**, *2*, 661−666.
(29) Rubinstein, M.; Colby, R. H., *Polymer Physics*; Oxford University Press: New York, NY, 2003.
(30) Flanders, M. J.; Gramlich, W. M. Reversible-addition fragmentation chain transfer (RAFT) mediated depolymerization of brush polymers. *Polym. Chem.* **2018**, *9*, 2328−2335.
(31) Dainton, F. S.; Ivin, K. J. Some thermodynamic and kinetic aspects of addition polymerization. *Q. Rev., Chem. Soc.* **1958**, *12*, 61−92.
(32) Dainton, F. S.; Ivin, K. J. Reversibility of the propagation reaction in polymerization process and its manifestation in the phenomenon of a 'ceiling temperature'. *Nature* **1948**, *162*, 705−707.
(33) Small, P. A. The equilibrium between methyl methacrylate and its polymer. *Trans. Faraday Soc.* **1953**, *49*, 441−447.
(34) Martinez, M. R.; Krys, P.; Sheiko, S. S.; Matyjaszewski, K. Poor solvents improve yield of grafting-through radical polymerization of OEO19MA. *ACS Macro Lett.* **2020**, *9*, 674−679.
(35) Bywater, S. Evaluation of heats and entropies of polymerization from measurements of equilibrium monomer concentration in solution. *Die Makromol. Chem.* **1962**, *52*, 120−124.
(36) Ivin, K. J.; Léonard, J. The effect of polymer concentration on the equilibrium monomer concentration for the anionic polymerization of a-methyl styrene in tetrahydrofuran. *Eur. Polym. J.* **1970**, *6*, 331−341.
(37) Fiscer, H. The persistent radical effect in "living" radical polymerization. *Macromolecules* **1998**, *30*, 5666−5672.
(38) Zhong, M.; Matyjaszewski, K. How fast can a CRP be conducted with preserved chain end functionality? *Macromolecules (Washington, DC, U. S.)* **2011**, *44*, 2668−2677.
(39) Dobrynin, A. V.; Carrillo, J. M. Y. Universality in nonlinear elasticity of biological and polymeric networks and gels. *Macromolecules* **2011**, *44*, 140−146.
(40) Braunecker, W. A.; Tsarevsky, N. V.; Gennaro, A.; Matyjaszewski, K. Thermodynamic components of the atom transfer radical polymerization equilibrium: quantifying solvent effects. *Macromolecules* **2009**, *42*, 6348−6360.
(41) Lee, J. N.; Park, C.; Whitesides, G. M. Solvent compatibility of poly(dimethylsiloxane)-based microfluidic devices. *Anal. Chem.* **2003**, *75*, 6544−6554.
(42) Tang, W.; Kwak, Y.; Braunecker, W.; Tsarevsky, N. V.; Coote, M. L.; Matyjaszewski, K. Understanding atom transfer radical polymerization: effect of ligand and initiator structures on the equilibrium constants. *J. Am. Chem. Soc.* **2008**, *130*, 10702−10713.
(43) Tang, W.; Matyjaszewski, K. Effects of initiator structure on activation rate constants in ATRP. *Macromolecules (Washington, DC, U. S.)* **2007**, *40*, 1858−1863.
(44) Lin, C. Y.; Coote, M. L.; Petit, A.; Richard, P.; Poli, R.; Matyjaszewski, K. Ab Initio study of the penultimate effect for the ATRP activation step using propylene, methyl acrylate, and methyl methacrylate monomers. *Macromolecules* **2007**, *40*, 5985−5994.
(45) Matyjaszewski, K. Atom transfer radical polymerization (ATRP): current status and future perspectives. *Macromolecules* **2012**, *45*, 4015−4039.
(46) Konkolewicz, D.; et al. Aqueous RDRP in the presence of Cu^0: the exceptional activity of Cu^I confirms the SARA ATRP mechanism. *Macromolecules* **2014**, *47*, 560−570.
(47) Konkolewicz, D.; et al. SARA ATRP or SET-LRP. End of controversy? *Polym. Chem.* **2014**, *5*, 4396−4417.
(48) Ribelli, T. G.; Krys, P.; Cong, Y.; Matyjaszewski, K. Model studies of alkyl halide activation and comproportionation relevant to RDRP in the presence of Cu0. *Macromolecules* **2015**, *48*, 8428−8436.
(49) Matyjaszewski, K.; Paik, H.; Zhou, P.; Diamanti, S. J. Determination of activation and deactivation rate constants of model compounds in atom transfer radical polymerization. *Macromolecules* **2001**, *34*, 5125−5131.
(50) Martinez, M. R.; Cong, Y.; Sheiko, S. S.; Matyjaszewski, K. Thermodynamic Roadmap for the Grafting-through Polymerization. *ACS Macro Lett.* **2020**, *9*, 1303−1309.
(51) Maksym, G. N.; Bates, J. H. T. A distributed nonlinear model of lung tissue elasticity. *J. Appl. Physiol.* **1997**, *82*, 32−41.
(52) Savin, T.; et al. On the growth and form of the gut. *Nature* **2011**, *476*, 57−62.
(53) Annaidh, A. N.; Bruyère, K.; Destrade, M.; Gilchrist, M. D.; Otténio, M. Characterization of the anisotropic mechanical properties of exercised human skin. *J. Mech. Behav. Biomed. Mater.* **2012**, *5*, 139−148.
(54) Jabareen, M.; Mallik, A. S.; Bilic, G.; Zisch, A. H.; Mazza, E. Relation between mechanical properties and microstructure of human fetal membranes: an attempt towards a quantitative analysis. *Eur. J. Obstet. Gynecol. Reprod. Biol.* **2009**, *144*, 5134−5141.
(55) Zhou, B.; Xu, F.; Chen, C. Q. Strain rate sensitivity of skin tissue under thermomechanical loading. *Phil. Trans. R. Soc.* **2010**, *368*, 679−690.

https://dx.doi.org/10.1021/acs.macromol.0c01083
Macromolecules 2020, 53, 8324−8332

(56) Hou, C.; et al. Synthesis of poly(2-hydroxyethyl methacrylate) end-capped with asymmetric functional groups *via* atom transfer radical polymerization. *New J. Chem.* **2014**, *38*, 2538−2547.

https://dx.doi.org/10.1021/acs.macromol.0c01083
Macromolecules 2020, 53, 8324−8332